JOURNAL OF AIRCRAFT
Vol. 33, No. 1, January–February 1996

Introductory Analysis of Boundary-Layer Development on De/Anti-Icing Fluid

E. Perron,* P. R. Louchez,† and J. L. Laforte‡
Université du Québec à Chicoutimi, Chicoutimi, Quebec G7H 2B1, Canada

When aircraft are kept on the ground for a significant period of time under cold precipitation, anti-icing fluids are used to prevent ice buildup. Unfortunately, at the time of takeoff, the residual fluid on wings modifies the boundary layer of the air and causes lift loss. The purpose of this work was to study the boundary-layer development of the air flowing above a horizontal flat plate covered with a de/anti-icing fluid film. The objective was to find the relationship between the air boundary layer and the geometric and dynamic characteristics of the air/fluid interface. This work consists of numerical and experimental studies. The experimental work contains a rheological study of the fluid and wind-tunnel tests on flat plates in order to describe the movement of the fluid during airflow acceleration. The numerical modeling is used for the prediction of the wave characteristics at the interface and for the determination of the integral relationships for rough boundary-layer conditions. The model of stability gave a good correlation between theory and experiment for the waveform at the air/fluid interface. A simple integral model determines an equivalent flat plate roughness that produces the same boundary layer as with the fluid. This equivalent roughness corresponds, in general, to the waveform, which indicates that the influence of the fluid seems to be only geometrical in nature.

Nomenclature

A = constant of viscosity function, Pa·s^m
C_f = local friction coefficient
$C_{L\max}$ = maximum lift coefficient
c = phase velocity (complex number), m/s
d = mean fluid thickness, m
d' = wave height, m
e = local fluid thickness, m
Fr = Froude number
f = velocity profile without core wake
h = duct height, m
I = light intensity
I_0 = incident light intensity
K = von Kármán constant
k_g = geometric roughness height, m
k_s = sand grain roughness height, m
m = power of viscosity function
P = static pressure, Pa
p = harmonic pressure solution
Re = Reynolds number
r = density ratio
T = surface tension, N/m
U = velocity in x direction, m/s
u_* = friction velocity, m/s
w = test duct width, m
x = horizontal flat plate distance, m
y = height over a fluid film, m
y_* = friction height, m
α = wave number, m^{-1}
β = absorption coefficient, m^{-1}
$\dot{\gamma}$ = shear rate, s^{-1}
δ = boundary-layer thickness, m
δ^* = boundary-layer displacement thickness, m
δ_d^* = dry boundary-layer displacement thickness, m
δ_f^* = measured boundary-layer displacement thickness, m
θ = momentum thickness, m
λ = calculated wavelength, m
λ_s = interspacing between waves, m
μ = dynamic viscosity, Pa·s
ν = kinematic viscosity, m^2/s
Π = Cole's wake function
ρ = density, kg/m^3
σ = growth rate of wave
τ = shear stress, Pa
ϕ = harmonic velocity solution, m^2/s
ψ = dimensionless stream function

Subscripts
a, f, ∞ = air, fluid, and freestream, respectively
θ, x, d = momentum thickness, position on a plate, and fluid thickness, respectively
1, 2, 3 = correspond to measurements location along the flat plate

Superscript
$\sim$ = dimensionless values

I. Introduction

IN winter, aircraft on the ground can be subjected to ice contamination due to freezing precipitation adhering to the surface. In these conditions, the aircraft cannot takeoff safely because the pressure distribution around the wings is perturbed by the ice, which results in a lift loss.[1,2] To solve this problem, de-icing and anti-icing fluids have been developed. These fluids are water–glycol compounds with additives. The de-icing fluids are low viscosity, Newtonian fluids used to remove the ice on aircraft. The anti-icing fluids are high-viscosity, pseudoplastic fluids used to prevent ice buildup while the aircraft waits on the ground before takeoff. When applied on the aircraft body these fluids form a thick protective film and during ground acceleration flow off the surface as a result of viscosity reduction due to pseudoplastic effect at high shear rate. In recent years anti-icing fluids have started to be used without further cleaning procedure prior to takeoff; this is an exception to the clean wing rule required otherwise. Despite the pseudoplastic behavior, the fluid is not to-

Received Aug. 8, 1994; revision received July 1, 1995; accepted for publication July 12, 1995.
*Graduate Student. Student Member AIAA.
†Professor, Department of Applied Sciences. Member AIAA.
‡Professor, Department of Applied Sciences.

tally eliminated when the wheels of the aircraft leave the ground. Consequently, the residual fluid is a new contaminant and the lift perturbation appears again. For safe operation, the lift loss at $C_{L_{max}}$ due to the fluid, must remain below about 5% for large aircraft (B737, DC10, and A320, etc.[3,4]).

II. Flow-Off of Anti-Icing Fluids

The lift modification depends on the dynamic and geometric characteristics of the boundary layer. It has been shown[5] that the boundary-layer thickness developed on a horizontal flat plate covered by a film of anti-icing fluid can be correlated with the lift loss. More precisely, the measure of the boundary-layer displacement thickness (BLDT), at the end of the plate with a length equivalent to the wing chord, was shown to be proportional to the lift loss measured in a wind tunnel on a two-dimensional wing. A mathematical definition of the BLDT, δ^*, is given in Eq. (1), depending on the boundary-layer thickness and the freestream velocity:

$$\delta^* = \int_0^{\delta} \left(1 - \frac{U}{U_\infty}\right) \cdot dy \tag{1}$$

Consequently, the evaluation of the safety at takeoff in the presence of the residual anti-icing fluid on the wings may be obtained by measure of the BLDT developed on a fluid film applied on the horizontal flat plate under a pertinent acceleration.[6]

The cost of the experimental procedures and the variability of the real conditions have recently moved the research towards the numerical prediction of the aerodynamic effects at takeoff due to the pseudoplastic fluid film. The first step of the research consists of deriving the BLDT on a flat plate situation. At the moment, the problem of the air turbulent boundary layer on a pseudoplastic fluid film has not been studied and information on the perturbation caused by an air/fluid interface is limited. A comparison made by Carbonaro[2] with classical results on solid roughness shows that the roughness at the interface created by the instability of the fluid can be, in part, responsible for the BLDT amplification. The presence of the fluid film on a wing can multiply the BLDT by a factor of four. However, presently, it is not known to what extent the roughness created by the waves at the interface is responsible for the BLDT value.

This study is a contribution to the development of methods to predict lift loss induced by the presence of the residual fluid film on the wing during takeoff with respect to fluid characteristics. This work is based on numerical and experimental studies. The experimental work consists of a rheological study of the fluid and wind-tunnel tests on a flat plate in order to describe the movement of the fluid during airflow acceleration. All experimental measurements presented in this article are performed in the facilities of the Anti-Icing Materials International Laboratory (AMIL) operated by the Groupe de Recherche en Ingénierie de l'Environnement Atmosphérique (GRIEA) at the Université du Québec à Chicoutimi (UQAC).

The modeling work is composed of two different aspects. First, it consists of predicting the wave characteristics at the air/fluid interface using Yih's stability analysis.[7] The second aspect corresponds to the determination of the integral relationships for rough boundary-layer conditions that permit the evaluation of the equivalent roughness created by waves on a fluid covered flat plate.

In this work, two typical commercial fluids are used to illustrate the general anti-icing fluid behavior. Fluids are designated by the AMIL code. Identification and detailed formulation of the fluids are proprietary information, and therefore, restricted. However, the viscosity data, given later on, will provide sufficient definition of the fluids for the purpose of the present work. The fluid A-409 is studied at -10 and 20°C and the fluid A-447 at -20°C. For each flow-off elimination, two pertinent cases, during takeoff, will be examined. The first case corresponds to a few seconds after wind acceleration (at about 20–26 m/s). This case corresponds to the instant of large waves generation at the air/fluid interface. The second case corresponds to the time when the wheels of the aircraft leave the ground, typically 30 s after the start of wind acceleration (at about 65 m/s).

III. Experimental Results

A. Measurement of Pseudoplastic Rheology

Anti-icing fluids are non-Newtonian and they have a pseudoplastic behavior to keep high viscosity at low shear rate and low viscosity at high shear rate. This property provides a thick protective film while the aircraft is waiting to take off and a good elimination during the ground acceleration. Rheological measurements are thus required to determine the correspondence between viscosity and shear rate.

The viscosity is measured with a coaxial viscometer. The shear rate varies with the rotation speed and the dimension of the spindle. The shear stress is obtained from the torque measurement.

For a pseudoplastic fluid, the relation between shear stress and shear rate is presented in Eq. (2), and the viscosity in function of the shear rate in Eq. (3):

$$\tau = A\dot{\gamma}^m \tag{2}$$

$$\mu = A\dot{\gamma}^{m-1} \tag{3}$$

The constants A and m for the fluid A-409 are $A = 0.57$ Pa·s^m, $m = 0.50$ at 20°C, $A = 1.08$ Pa·s^m, $m = 0.43$ at -10°C; and for the fluid A-447 at -20°C, $A = 1.39$ Pa·s^m, $m = 0.81$. Figure 1 shows the relationship between viscosity and shear rate for the typical fluid at 20°C.

B. Boundary-Layer Measurements

The closed-circuit, refrigerated, wind tunnel at the AMIL laboratory has a test section 50 cm wide, 60 cm high, and 1.5 m long. The overall circuit length is about 30 m. The fan is

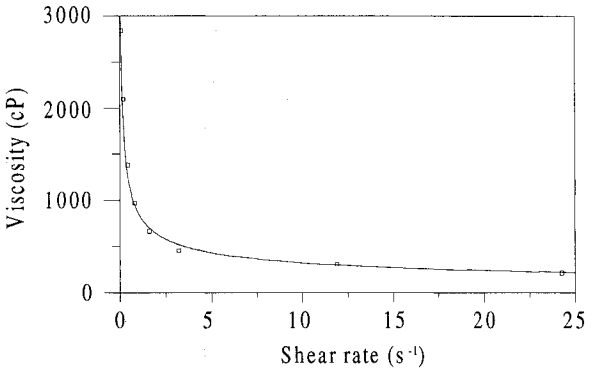

Fig. 1 Viscosity variation with shear rate.

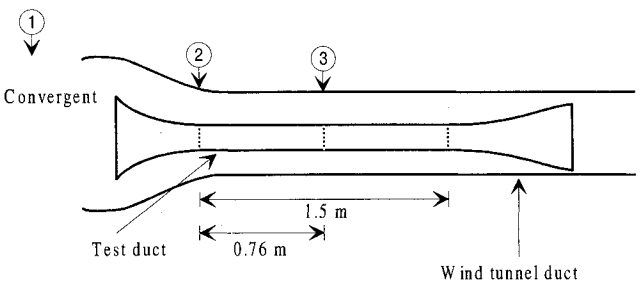

Fig. 2 Test section of the wind tunnel.

powered by a 50-hp ac motor drive and can provide a velocity up to 70 m/s. A detailed description of this setup is given in Ref. 8. The horizontal flat plate is the bottom of a test duct inserted in the test section of the wind tunnel. The test duct has a movable top for application and cleaning of the fluid (see Fig. 2). An elimination test is a standard procedure discussed in detail in Ref. 8. Its purpose is the study of the flow-off of a 2-mm fluid film applied on the flat bottom plate of the test duct. Two steps are performed in the elimination test. The first step is an acceleration of approximately 2.6 m/s^2 while the air velocity passes from 0 to 65 m/s (about 30 s) and the second step consists of steady airflow at 65 m/s during 30 s. An acquisition system records the pressure and temperature outputs in the duct during the air acceleration. The pressure measurement at the entrance and the end of the duct allows the calculation of the BLDT. The static pressure drop in the duct is related to the BLDT value according to Eq. (4) (see Ref. 8):

$$\delta_f^* = F_A - F_B \cdot \delta_d^* - F_C \sqrt{\frac{(P_1 - P_2)}{(P_1 - P_2) + (P_2 - P_3)}} \quad (4)$$

where

$$F_A = h_3, \qquad F_B = 1 + \frac{2h_3}{w_3}, \qquad F_C = \frac{h_2 \cdot w_2}{w_3}$$

and δ_d^* is a dry BLDT (without fluid) and locations 1, 2, and 3 are shown on Fig. 2. The test duct dimensions h_2, h_3, w_2 and w_3 are given in Table 1.

Table 1 Test duct dimensions

	X position, m	w, mm	h, mm
②	0.08	303.30	100.90
③	0.76	303.30	106.02

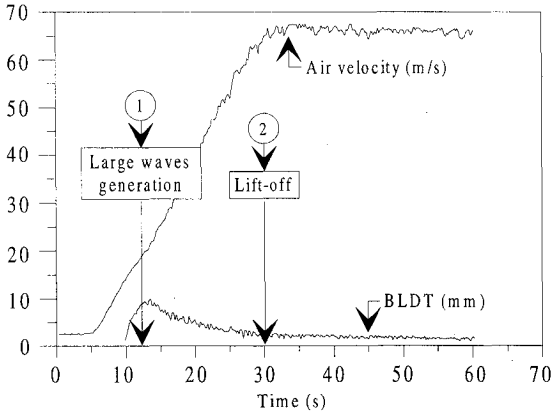

Fig. 3 Typical flat plate data.

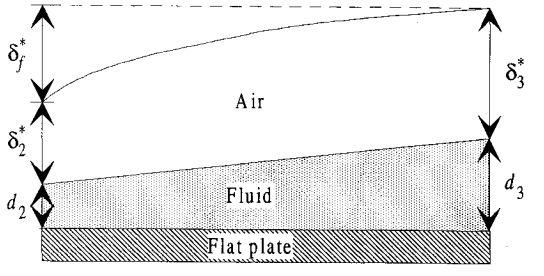

Fig. 4 Definition of thicknesses.

Figure 3 shows a typical result of BLDT development with anti-icing fluid. As explained in Fig. 4, the true value of the BLDT at location 3, δ_3^*, is related to the measured BLDT value, δ_f^*, and other thickness by the following equation:

$$\delta_3^* = \delta_f^* + (d_2 + \delta_2^*) - d_3 \quad (5)$$

To isolate δ_3^*, the knowledge of the average fluid thickness for the two positions (d_2 and d_3) is thus required. This is given by image analysis. The BLDT at position 2 (δ_2^*) is estimated by integral relationships and is given in Table 2 for the various cases studied.

C. Validation of Blockage Method by Hot-Wire Anemometry

Because of the presence of a liquid interface, the blockage method, detailed before, is chosen for measurement of fluid-induced BLDT. A hot-wire anemometer is used to validate this blockage method. This is done by the study of the boundary layer induced over a rough solid surface, where the BLDT value, directly derived from the velocity profile obtained by hot-wire measurement, can be compared to the blockage method value. After calibrating the hot wire according to standard procedure, the air velocity profile is measured at the same streamwise position as that of the pressure sensor (at 1.5 m). The data are fitted by a least-square method and then integrated to provide the BLDT value. The BLDT validation is performed for two cases with air velocity at 65 m/s. The first case corresponds to the smooth flat plate and the second is the sandpaper roughness case of about 0.2 mm. The velocity profile measured with hot-wire anemometer for the sandpaper is shown in Fig. 5. Comparison of BLDT values based on velocity profile integration and the BLDT by blockage method for the smooth and rough situations at 65 m/s are shown in Table 3. Results indicate that the BLDT value measured by

Table 2 Thickness measurement and BLDT evaluation at location 2

Fluid	Temperature, °C	U_∞, m/s	d_2, mm	δ_2^*, mm
A-409	20	18.54	0.094	0.36
A-409	20	65.00	0.039	0.28
A-409	−10	26.86	0.150	0.33
A-409	−10	65.68	0.150	0.28
A-447	−20	25.89	0.150	0.33
A-447	−20	65.43	0.150	0.28

Table 3 Comparison of BLDT measurement methods

	Blockage, mm	Hot wire, mm
Smooth	2.69	2.70
Rough	5.88	5.84

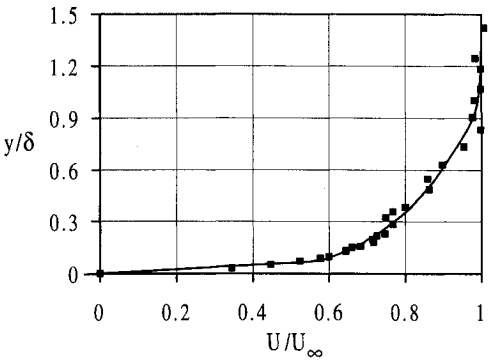

Fig. 5 Rough turbulent mean velocity profile.

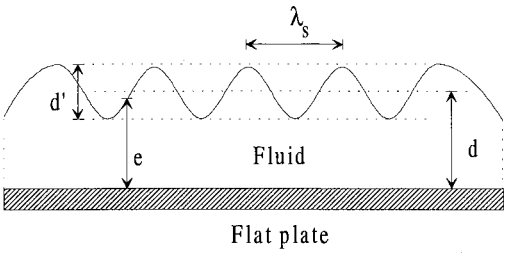

Fig. 6 Definition of wave geometrical parameters.

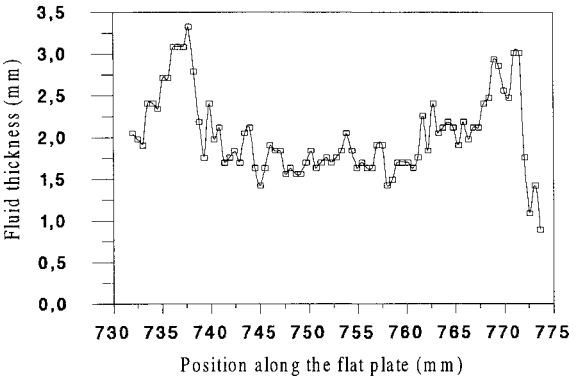

Fig. 7 Example of fluid thickness (A-409 at 20°C at 12.1 s).

the blockage method yields good agreement with the measurements based on velocity profile.

D. Surface Description by Image Analysis

An IR video camera, placed above the test section, can record images at a rate of 60 images/s for postimage analysis. The image analysis of the video in IR, taken during the elimination test, allows the fluid thickness determination for situations of interest during the air acceleration. The video photographs were digitized and the gray levels were converted into the thickness value using the Beer–Lambert law for I:

$$I = I_0 \exp^{-\beta e} \tag{6}$$

The constant β is determined by calibration and includes the dye concentration of the fluid. The fluid is colored with Pyronin B and presents a good absorption of the incident light intensity in IR spectrum. Figure 6 shows the representation of the various geometrical parameters of surface: the local fluid thickness, the average fluid thickness, the peak-to-peak value, and the wavelength. Figure 7 shows an actual thickness two-dimensional profile at 12.1 s (first case of interest) for the fluid A-409 at 20°C. The wave characteristics measured for various cases: height parameters d and d', and spacing parameters λ_s and Λ (to be defined later) are presented in Table 4. It should be noted that the accuracy in height measurement (d and d') is about ± 0.02 mm for A-409 at 20°C. However, due to noise-filtering problems, in other cases the accuracy significantly dropped to about ± 0.20 mm.

IV. Analytical Details

A. Calculation of Wavelength by Stability Analysis

The interest of the parallel flow stability analysis is the prediction of the wavelength (wave interspacing) generated by the airflow over the anti-icing fluid film. The stability analysis predicts also when the first wave can appear. This information is obtained from the study of the growth rate of perturbation at a given wave number. The calculation method for growth rate has been developed by Yih[7] and is summarized hereafter. The situation is a double-layer flow, air and fluid, separated by an interface where the wave perturbs the velocity

Table 4 Experimental and numerical data for the two reference cases (at position 3)

	A-409 at 20°C		A-409 at −10°C		A-447 at −20°C	
	①	②	①	②	①	②
Time, s	12.1	30.5	15.0	30.0	15.0	30.0
U_∞, m/s	18.54	65.0	26.86	65.68	25.89	65.43
δ^*, mm	8.61	2.18	4.67	3.67	6.49	4.40
d, mm	1.84	0.54	1.1	0.5	2.0	0.5
Λ	4.63	2.26	5.0	4.0	5.0	4.0
λ_s, mm	31.0	3.3	10.0	3.0	20.0	3.5
λ, mm[a]	20.82	3.25	10.35	3.15	12.60	3.11
d', mm	1.16	0.28	0.8	0.5	1.1	0.5
k_g, mm[a]	1.39	0.30	0.85	0.43	0.85	0.43
$\dot{\gamma}$, s^{-1}	29.7	346.5	17.5	469.1	6.2	35.0
μ, cP	110	30	280	40	980	780
τ, Pa	3.1	10.7	5.0	20.7	6.1	24.7

[a]Values calculated from boundary-layer integration and experimental data.

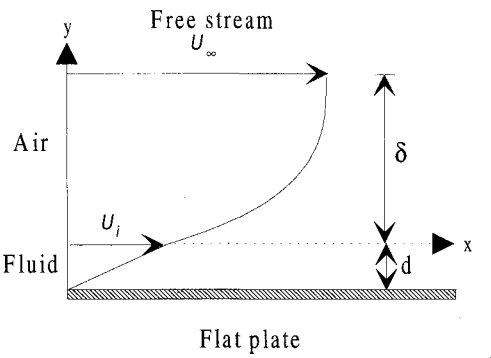

Fig. 8 Definition of double-layer velocity distribution.

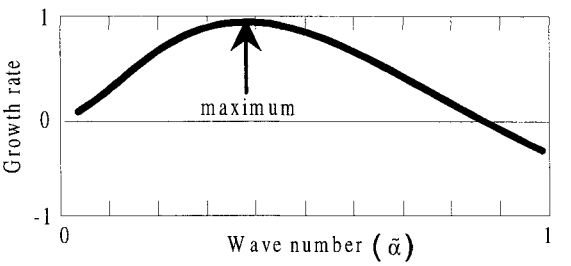

Fig. 9 Typical growth rate variation with wave number.

and pressure in each flow (see Fig. 8). Circular harmonic perturbations of the stream function and the pressure fluctuation are defined as follows:

$$\tilde{\psi} = \phi(\tilde{y})\exp[i\tilde{\alpha}(\tilde{x} - \tilde{c}\tilde{t})] \tag{7}$$
$$\tilde{p}' = p(\tilde{y})\exp[i\tilde{\alpha}(\tilde{x} - \tilde{c}\tilde{t})]$$

where $\tilde{\alpha}$ is the dimensionless wave number based on fluid thickness and wavelength: $\tilde{\alpha} = 2\pi d/\lambda$; $\tilde{c} = \tilde{c}_r + i\tilde{c}_i$ is the phase velocity, and $\sigma = \tilde{\alpha}\tilde{c}_i$ is the growth rate. The introduction of these definitions into the Navier–Stokes equations, after linearization, gives the Orr–Sommerfeld equations, for air and fluid fields. The application of the boundary conditions gives the complex Eq. (8) (see Ref. 7).

$$\frac{b^2\mu_f\tilde{c}}{\mu_a Re_d} = \left\{\frac{Q}{L} - b^2[(r-1)Fr^{-2} + \tilde{\alpha}^2 S]\right\} \times \left\{\frac{\sinh(\tilde{\alpha})\cosh(\tilde{\alpha}) - \tilde{\alpha}}{2\tilde{\alpha}^2[\cosh^2(\tilde{\alpha}) + \tilde{\alpha}^2]}\right\} \tag{8}$$

where

$$Q = (1 - \eta)(i + 3\xi\tilde{\alpha}^2\varepsilon^2) - \frac{2\tilde{\alpha}}{Re_d}[1 - \tilde{\alpha}b(1 + \eta)]$$

$$L = b^{-1} - \tilde{\alpha}(1 + \eta) + [-\xi\varepsilon^{-1}(1 - \eta)]$$

$$b = \left(\frac{\partial \tilde{U}_{\text{air}}}{\partial \tilde{y}}\bigg|_{\tilde{y}=0} \cdot d\right)^{-1}, \qquad \varepsilon = \left(\frac{b}{\tilde{\alpha} Re_d}\right)^{1/3}$$

$$\xi = -(1.1155 + 0.6440i), \qquad \eta = \frac{1}{2\tilde{\alpha}b}(1 - \exp^{-2\tilde{\alpha}b})$$

$$S = \frac{T}{\rho_a U_\infty^2 d} \quad \text{and} \quad r = \frac{\rho_f}{\rho_a}$$

The imaginary part of Eq. (8) gives the growth rate of the perturbation and the real part gives the phase velocity. A typical growth rate in function of the wave number is shown in Fig. 9. The wave number at the maximum growth rate is expected to correspond to the observed wave. In Table 4 λ, calculated with Eq. (8), are listed for the typical anti-icing fluids and the two situations of interest. These theoretical results are in agreement with λ_s, obtained by the image analysis for the same conditions (Table 4).

B. Calculation and Role of Surface Roughness

As usual, the basic geometrical parameter of the boundary layer used for calculation is the momentum thickness defined by

$$\theta = \int_0^\delta \frac{U}{U_\infty}\left(1 - \frac{U}{U_\infty}\right) dy \tag{9}$$

We introduce the friction velocity and the friction height from the air surface shear stress

$$\tau_a = \rho_a u_*^2 = \rho_a \nu_a^2 / y_*^2 \tag{10}$$

The rough turbulent profile can be defined as

$$\tilde{U}/u_* = f(y/y_*) + \Pi(Re_\theta)\cdot \sin^2(\pi/2)\cdot(y/\delta) \tag{11}$$

with

$$f(y/y_*) = (1/K)\cdot \ln(y/y_*) - (1/K)\ln(k_s/y_*) + 8.48 \tag{12}$$

where $Re_\theta = U_\infty \theta/\nu_a$ and k_s is the equivalent sand grain roughness of the surface. A numerical scheme allows the determination of the equivalent sand grain roughness corresponding to the experimental BLDT on the flat plate covered by anti-icing fluid. The dimensionless numbers of the problem are Re_x, Re_θ, δ/y_*, and u_*/U_∞. The basic equations of the problem are the von Kármán, Eq. (13), the friction law (taking $y = \delta$ in the velocity profile), Eq. (14), and the momentum thickness definition (using the velocity profile), Eq. (15):

$$\frac{dRe_\theta}{dRe_x} = \left(\frac{u_*}{U_\infty}\right)^2 \tag{13}$$

$$\frac{u_*}{U_\infty} = \frac{1}{f(\delta/y_*) + \Pi(Re_\theta)} \tag{14}$$

$$Re_\theta = \left(I_1 - I_2 \frac{u_*}{U_\infty}\right) + \left\{\frac{1}{2}\frac{\delta}{y_*}\Pi(Re_\theta) - \frac{3}{8}[\Pi(Re_\theta)]^2 \frac{u_*}{U_\infty}\frac{\delta}{y_*}\right\} \tag{15}$$

where

$$I_1 = \int_0^{\delta/y_*} f(q)\cdot dq \quad \text{and} \quad I_2 = \int_0^{\delta/y_*} f^2(q)\cdot dq$$

Equations (13–15) form an integro-differential system that is solved to calculate δ/y_*, u_*/U_∞, and Re_θ parameters for a given Reynolds number Re_x. Then, δ^* and C_f can be evaluated according to Eqs. (16) and (17):

$$\delta^* = \frac{x}{Re_x}\left(\frac{U_\infty}{u_*}\right)\left[\frac{\delta}{y_*} - \frac{u_*}{U_\infty} I_1 - \frac{\Pi(Re_\theta)}{2}\frac{\delta}{y_*}\right] \tag{16}$$

$$C_f = 2(u_*/U_\infty)^2 \tag{17}$$

The validation of the integration was performed against the well-known Schlichting formula for C_f for a solid k_s:

$$C_f = [2.87 + 1.58 \log(x/k_s)]^{-2.5} \tag{18}$$

Comparison of our integration scheme with the Schlichting formula for sand roughness yields good agreement for C_f data (typically above $Re_x = 10^6$). An example is shown in Fig. 10 with $k_s/y_* = 500$.

The algorithm presented so far enables us to calculate k_s, which produces a boundary-layer profile equivalent to that of fluid interface. To compare with actual wave height, the spacing factor has to be taken into account; i.e., k_s must be converted into an equivalent k_g, which has the same spacing as the waves. Evaluation of k_g can be done according to the Betterman[9] correlation:

$$(1/K)\ln(k_g/k_s) + 2.98 = 17.35 \times (0.706 \ln \Lambda - 1) \quad \text{for} \quad 1 \le \Lambda \le 5 \tag{19}$$

$$(1/K)\ln(k_g/k_s) + 2.98 = -5.85 \times (0.479 \ln \Lambda - 1) \quad \text{for} \quad \Lambda \ge 5 \tag{20}$$

where Λ is the roughness density parameter. This parameter is derived from image analysis by calculating the ratio of the total surface area to the roughness area measured at midheight of the wave; in this fashion, the roughness density parameter based on surface roughness is about equal to the roughness density parameter based on the frontal area which, according to Simpson,[10] provides a better definition for Λ. From the Λ value, and with the k_s, we can evaluate the equivalent k_g. Result accuracy depend on the noise level in image analysis which, as noted before, was much better for A-409 at 20°C than for other cases. In this case, Λ is estimated at ± 0.02 mm, λ at ± 0.1 mm, and the resulting k_g at ± 0.02 mm. For other cases we have Λ at ± 0.5 mm, λ at ± 0.2 mm, and the

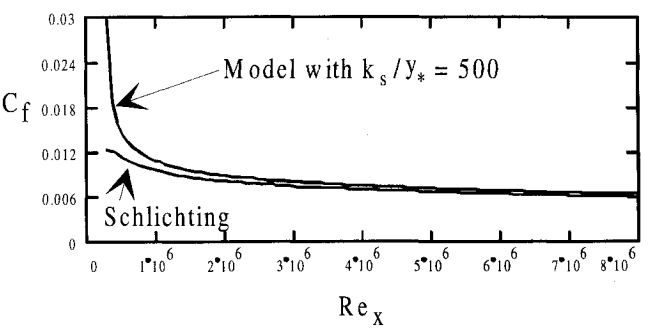

Fig. 10 Validation of integration scheme for rough turbulent boundary layer.

resulting k_g at ± 0.1 mm. All results are listed in Table 4. Comparison of actual fluid roughness with equivalent solid roughness can be done on the basis of the elements interspacing (λ vs λ_s) and elements height (d' vs k_g). For the two situations examined here, the order of magnitude is equivalent for solid and fluid roughness. Similar parameters are in agreement within about 10%, with two exceptions for interspacing and one exception for height (both in case ①). It is therefore fair to assume that the movement of the wave does not have a specific influence on the air boundary layer since fluid interface has the same effect as a solid roughness.

At this time the amount of data is too limited to derive a reliable interpretation of the role of the fluid rheology on the generation of wave roughness. However, some comments can be made at this point. Warm fluid tends to generate a larger perturbation than cold fluids (see A-409 at 20°C and −10°C). This may be the direct consequence of the higher viscosity at lower temperature that is damping fluid instability. At high shear, it can be seen that the tendency is reversed, probably as a result of that larger pseudoplastic effect on warm fluid.

C. Evaluation of Fluid Shearing Stress

Using a simple assumption of linear velocity profile in the fluid, the shear stress in the fluid is constant and equal to its value at the air/fluid interface. The tangential force equilibrium at the interface (neglecting surface tension) requires that, at the interface

$$\tau_a = \tau_f \tag{21}$$

Thus, it suffices to calculate the shear stress in the air layer, at the air/fluid interface, to obtain the fluid shearing stress. The shear stress in the air during the airflow acceleration can be calculated by

$$\tau_a = \tfrac{1}{2}\rho U_\infty^2 C_f \tag{22}$$

where C_f is calculated by the program described in Sec. IV.B, with the B constant scaled by the BLDT measurement. Following our rheological studies (Sec. III.A), the relation between viscosity and shear rate is known, we can thus obtain the corresponding viscosity. The results are presented in Table 4 for the two specific flow conditions with typical anti-icing fluids.

These values are of particular significance since they scale the level of shearing experienced during takeoff, which can be compared to the level of shearing applied during viscosity measurement required for standard evaluation.[11] To produce the same level of shearing in the fluid, as during the airflow acceleration, a high rotation of the viscometer is required. At the end of takeoff, the level of shear is much larger than that obtained with the maximum speed required in standard viscosity measurement (60 rpm). This is consistent with the industrial practice of using low rpm pumps to apply anti-icing fluids (contrary to high-pressure pumps for de-icing fluids).

V. Conclusions and Future Work

The experimental and numerical studies presented in this work allow a better understanding of the fluid behavior during ground acceleration of large aircraft at takeoff. The stability analysis (scaled by fluid thickness and viscosity) allows the evaluation of (with good precision) the wavelength of the wave at the air/fluid interface. This same analysis defines the air velocity at the air/fluid interface. The first waves appear at approximately 8 m/s. For lower velocity (corresponding to taxiing situations) the shear stress created by the airflow is not sufficient for wave generation, the fluid thickness is not varying significantly, and the fluid stays on the wing. At this time the fluid is very viscous and ice protection is good. The acceleration between 15–50 m/s corresponds to the major fluid elimination process. At this moment, the large waves create a mass flow of the fluid and the BLDT perturbation is very high. In this stage, the roughness created by the waves increases the shear stress and stimulates the shear thinning behavior of the fluid (pseudoplastic) and a low fluid viscosity appears. At the end of this stage, only a residual fluid film stays on the wing and the thickness and waveform at this moment are very important because the aircraft takeoff velocity is around 65 m/s and the fluid influence is critical at this point. This is the situation that is used for the standard ASTM acceptance tests for anti-icing fluid.

The roughness analysis using an integration of the rough turbulent boundary layer demonstrates that the air/fluid interface effect is only geometrical and the movement of the wave does not have a significant effect on boundary-layer development. Thus, the boundary-layer development over a fluid film can be simulated by a solid roughness boundary layer on a flat plate with the same height and spacing as those of the waves. However, at this time, the wave analysis is not sufficient since it does not provide the height of the wave (only the interspacing).

The method developed in this work gives a better understanding of the fluid effects during aircraft takeoff, but is not complete since it does not permit the simulation of the boundary-layer development without the help of experimental data. A future challenge will be to obtain the wave height in function of the fluid characteristics. Then, a historical evolution of the roughness of the surface will have to be developed to provide a complete numerical description of the air boundary layer during acceleration over a pseudoplastic fluid.

Acknowledgments

This article was partially funded by the Natural Sciences and Engineering Research Council Grant OGP0039720 and by the Dryden Commission Implementation Project at Transport Canada. The authors are particularly indebted to the fluid manufacturers for providing the experimental fluids. The technical support of the AMIL where the experiments were performed is also gratefully acknowledged.

References

[1]Zierten, T. A., and Hill, E. G., "Effects of Wing Simulated Frost on Airplane Performance," von Kármán Institute for Fluid Dynamics Lectures Series, Influences of Environmental Factors on Aircraft Performance, VKILS 1987-3, Brussels, Belgium, Feb. 1987.

[2]Carbonaro, M., "Further Study of the Aerodynamic Performance of a Two-Dimensional Wing Model Covered with Simulated Frost or with De/Anti-Icing Fluid During a Wind Tunnel-Simulated Take-Off at Subfreezing Temperatures," von Kármán Inst. for Fluid Dynamics, Contract Rept. 1987-29, Brussels, Belgium, July 1987.

[3]Carbonaro, M., "Experimental Study of the Aerodynamic Characteristics of a Two-Dimensional Wing Model Covered with De/Anti-Icing Fluid During a Simulated Take-Off at Subfreezing Temperatures," von Kármán Inst. for Fluid Dynamics, Contract Rept. 1986-22, Brussels, Belgium, Aug. 1986.

[4]Runyan, L. J., Zierten, T. A., and Hill, G., "Flight and Wind Tunnel Investigation of Aerodynamic Effects of Aircraft Ground De-Icing/Anti-Icing Fluids," *Flight in Adverse Environmental Conditions* (Gol, Norway), CP 470, AGARD, 1989 (Paper 24).

[5]Hill, E. G., "Aerodynamic Acceptance Test for Aircraft Ground Deicing/Antiicing Fluids," Boeing Document D6-55573, Oct. 1990.

[6]Zierten, T. A., and Hill, E. G., "Wind Tunnel Investigation of the Aero-Dynamic Effects of Aircraft Ground De-Icing/Anti-Icing Fluids and Criteria for Aero-Dynamic Acceptance," AGARD FDP Specialist Meeting, Effects of Adverse Weather on Aerodynamics, Toulouse, France, April 1991.

[7]Yih, C. S., "Wave Formation on a Liquid Layer for De-Icing Airplane Wing," *Journal of Fluid Mechanics*, Vol. 212, 1990, pp. 41–53.

[8]Laforte, J. L., Louchez, P. R., and Bouchard, G., "Experimental Investigation of Boundary Layer over an Anti-Icing Fluid Film," *Canadian Aeronautics and Space Journal*, Vol. 39, No. 2, 1993, pp. 96–104.

[9]Betterman, D., "Contribution à l'Étude de la Couche Limite Turbulente le Long de Plaques Rugueuses," Laboratoire d'Aérothermique du CNRS, No. 65-6, 1965.

[10]Simpson, R. L., "A Generalized Correlation of Roughness Density Effects on the Turbulent Boundary Layer," *AIAA Journal*, Vol. 11, No. 2, 1973, pp. 242–244.

[11]"Aerospace Material Specifications De/Anti-Icing Fluid Aircraft," AMS 1424 Newtonian SAE type I and AMS 1428, Non-Newtonian Pseudo Plastic SAE type II, Jan. 1993.